Interfacial Charge-Transfer Loss in Dye-Sensitized Solar Cells

ARTICLE *in* THE JOURNAL OF PHYSICAL CHEMISTRY C · FEBRUARY 2013

Impact Factor: 4.77 · DOI: 10.1021/jp308193y

THE JOURNAL OF PHYSICAL CHEMISTRY C

Article

pubs.acs.org/JPCC

Interfacial Charge-Transfer Loss in Dye-Sensitized Solar Cells

Dong-Won Park,[†] Yonkil Jeong,*[,†] Jongjin Lee,[†] Jaeyoung Lee,[†,‡,§] and Seung-Hyeon Moon*[,‡]

[†]Research Institute for Solar and Sustainable Energies (RISE), [‡]School of Environmental Science and Engineering, and [§]Ertl Center for Electrochemistry and Catalysis, Gwangju Institute of Science and Technology (GIST), Gwangju 500-712, South Korea

ABSTRACT: Interfacial charge-transfer loss factors (CTLFs) of dye-sensitized solar cells (DSCs) were studied using a thermionic emission−diffusion theory and electrochemical impedance spectroscopy (EIS). It is found that the subsidiary CTLFs can be quantified including a native charge-transfer loss at the TiO_2/electrolyte interface in DSC devices. The obtained CTLFs as a probability parameter α were identified as almost matching to dominant resistance-capacitance (RC) time constants obtained from the EIS and its numerical calculation. The quantified CTLFs based on a detailed physical model of quantum-mechanical tunneling and reflection of charge carriers can explain a degradation of open-circuit voltage in DSC devices.

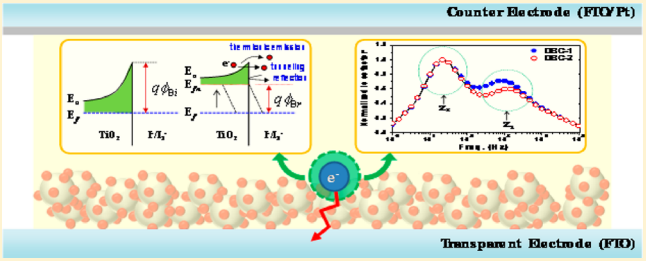

1. INTRODUCTION

Dye-sensitized solar cells (DSCs) have attracted great attention as an alternative to commercial bulk Si solar cells because of their low-cost manufacturability, simple fabrication process, available building-integrated photovoltaics, and robust thermal stability. However, the low efficiency of DSCs is still not free from competition with other alternatives.[1−6] A substantial understanding from the physical and chemical perspectives is necessary to achieve high efficiency in DSCs. Although many studies on device operation have been conducted since the advent of DSCs, a wider breadth of understanding is still necessary concerning the junction condition between semiconductors such as TiO_2 and electrolytes. An understanding of this condition both in equilibrium in darkness and in nonequilibrium under carrier injection, the potential barrier height of TiO_2 influencing the open-circuit voltage of DSCs, and charge carrier transport related to loss factors at the interfaces between the semiconductors and electrolytes and the metals and electrolytes is necessary.[7−12] Superficially, the device operation of DSCs appears to behave similarly to the general *p-n* junction devices, such as bulk Si solar cells.[13] However, the device structures of DSCs are different than general *p-n* junction devices, and their current−voltage characteristics also deviate from those of general *p-n* junction devices, which operate in diffusion and Shockley−Read−Hall (SRH) recombination dominant mode.[14] The device structure of DSCs has a nearly Schottky barrier structure, which implies that the device operation should be described by the thermionic emission of the charge carriers.[15] In addition, the energy band structure should be clarified for devices with diode characteristics in equilibrium under darkness or in nonequilibrium under carrier injection. For thermionic emission, an important carrier-transport process is the charge-transfer loss mechanism, which can be observed in a system consisting of TiO_2/electrolyte. However, the simple thermionic emission model is insufficient to comprehensively describe the device operation. A modified operation model is necessary to describe the charge-transport process between the physical behavior and the electrochemical reaction of charge carriers in a system consisting of TiO_2/electrolyte.

2. PRINCIPLES OF DEVICE OPERATION

2.1. General Principles of DSC Device Operation. The cells consist of a dye-adsorbed titanium dioxide and a counter electrode arranged in a sandwich configuration, as illustrated in Figure 1a. The interelectrode space is filled with an electrolyte containing a redox mediator. Figure 1b illustrates the general operation principles of DSC devices;[9,12,16−18] the dye molecules generate electrons after absorbing light ($D + h\nu \rightarrow D^*$), followed by the electron injection into the TiO_2 film ($D^* \rightarrow D^+ + e^-$). The oxidized dye is reduced to the neutral state by electron donation from an electrolyte containing the iodide/triiodide redox mediator ($2\,D^+ + 3I^- \rightarrow 2\,D + I_3^-$). At the counter electrode, the reduction of the triiodide to iodide is completed by drawing electrons from the external circuit ($I_3^- + 2e^- \rightarrow 3I^-$). However, undesirable side reactions are still present; the injected electrons may recombine with the oxidized sensitizer and/or with the oxidized redox couple at the TiO_2 surface, resulting in charge-transfer losses.

2.2. Thermionic Emission−Diffusion Theory for DSC Device Operation. The general diode equation is expressed by:

$$J = J_0 \exp\left(\frac{qV}{nkT} - 1\right) \sim J_0 \exp\left(\frac{qV}{nkT}\right) \quad (1)$$

where q/kT is the inverse thermal voltage, n is an ideality factor, and J_0 is the reverse saturation current density, which is regarded as a forward saturation current density in solar cells.

Received: August 17, 2012
Revised: November 26, 2012
Published: January 17, 2013

   dx.doi.org/10.1021/jp308193y | *J. Phys. Chem. C* 2013, 117, 2734−2739

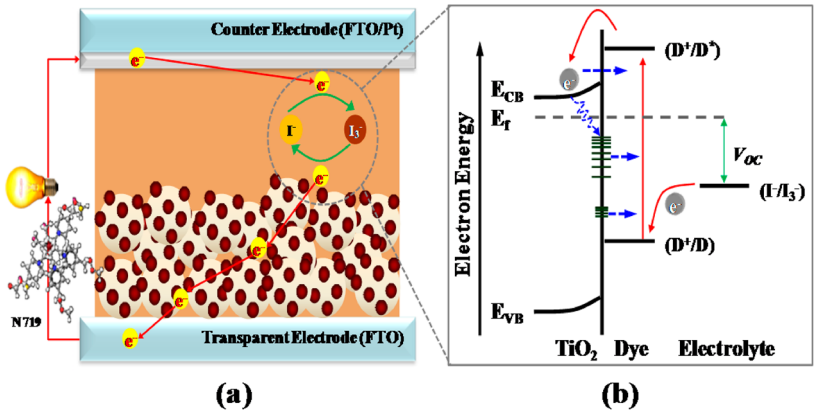

Figure 1. Schematics for the structure (a) and the general operation principles (b) of the DSCs. In panel b, the steps involved in the recombination between the photoinjected electron and the oxidized species in the electrolyte (dotted arrow) are shown.

The total current density of the Schottky barrier structure is similar to the transport equation for *p-n* junctions. However, the expressions for the reverse saturation current densities are quite different, as expressed by the following equation:[15]

$$J_0 = J_{00}\exp\left(-\frac{q\phi_B}{kT}\right) = A^*T^2\exp\left(-\frac{q\phi_B}{kT}\right) \quad (2)$$

where $q\phi_B$ is a Schottky barrier height, A^* is an effective Richardson constant, T is the absolute temperature, k is Boltzmann's constant, and J_{00} is a reverse saturation current density prefactor, which is regarded as a forward saturation current density prefactor in the solar cells. The effective Richardson constant is simply obtained by neglecting the crystal direction, as indicated in eq 3:

$$\left(\frac{A^*}{A}\right) \approx \frac{m^*}{m_0} \quad (3)$$

where A is the Richardson constant of 1.2×10^5 mA/cm^2/K^2 for free electrons, m_0 is the free electron mass, and m^* is the effective electron mass. The theory described above is a general thermionic emission theory for metal-semiconductor systems. The thermionic emission−diffusion (TED) theory is completed by synthesizing the Schottky's diffusion model and the Bethe's thermionic emission model, as indicated in eq 4:[19,20]

$$J_0 = J_{00}'\exp\left(-\frac{q\phi_{Bp}}{kT}\right) = \alpha A^*T^2\exp\left(-\frac{q\phi_{Bp}}{kT}\right) \quad (4)$$

where α is a TED parameter presenting the additional loss mechanism, as expressed in eq 5:

$$\alpha = \frac{1}{\frac{v_R}{v_D} + \frac{1}{f_P f_Q}} \quad (5)$$

where v_R is the thermionic recombination velocity, v_D is the effective diffusion velocity, f_P is the probability of electron emission over the maximum potential, and f_Q is the total current considering quantum-mechanical current flow.[13] Because f_P and f_Q are a probability and a ratio function, respectively, the parameter α is smaller than unity. The upper bound of α can be met when the denominator of eq 5 is unity. The parameter α can be quantitatively ranged in accordance with a loss mechanism.

In this work, the device physics of DSCs were investigated using a modified junction diode model with a Schottky barrier based on the TED process and electrochemical impedance spectroscopy (EIS). The TED-based diode junction model suggested in this work is applicable for describing the charge-transfer loss factors (CTLFs) in DSCs.[21] In addition, the parameter α obtained from the modified junction diode model was observed to be a physical quantity explaining the CTLFs caused at the TiO_2/electrolyte interface.

3. EXPERIMENTS

TiO_2 films were deposited using squeeze printing of a TiO_2 paste on FTO substrates (12 Ω/□, Pilkington) and annealing at 500 °C for 1 h. The titania paste was prepared by ball-milling TiO_2 powders (18 wt %; Degussa P25) with hydroxypropyl cellulose (5 wt %; Aldrich, $M_w \sim 80000$), terpineol (75 wt %; Aldrich), and lauric acid (2 wt %; Aldrich).[22,23] The as-calcined TiO_2 films were loaded overnight into a 0.5 mM ruthenium(II) dye (N719, Solaronix) ethanolic solution and then rinsed with anhydrous ethanol and air-dried at room temperature. These dye-adsorbed TiO_2 electrodes were assembled into solar cells with Pt-coated FTO glasses and a 3-methoxypropionitrile (Solaronix) electrolyte containing 0.6 M 1,2-dimethyl-3-propylimidazolium iodide (Solaronix), 0.5 M LiI (Aldrich), 0.05 M I_2 (Aldrich), and 0.5 M 4-*tert*-butylpyridine (Aldrich). The morphologies (particle size of appoximately 25 nm) and thicknesses (8−10 μm) of the TiO_2 electrodes were measured using field-emission scanning electron microscopy (FE-SEM; Hitachi, S-4700), as illustrated in Figure 2a,b. The conventional anatase phase of the TiO_2 film was confirmed using X-ray diffraction (XRD) (Figure 2c). Photocurrent−voltage measurements were performed for the active cell area of 0.25 cm^2 using a Keithley 4300 sourcemeter under 100 mW/cm^2 irradiation (Oriel, 96500 300 W solar simulator equipped with an AM 1.5G). To complement the photovoltaic characteristics of the DSSC, the EIS were investigated in the frequency range of 10^{-1} to 10^6 Hz with an a.c. amplitude of ±5 mV using a Electrochemical Workstation (CHI 660A, United States).

4. RESULTS AND DISCUSSION

Figure 3 presents the current density−voltage (*J-V*) characteristics of the DSCs under illumination. The DSC-1 exhibited the performance parameters with a short circuit current (J_{sc}) of 19.2 mA/cm^2, an open-circuit voltage (V_{oc}) of 0.69 V, a fill factor (FF) of 60.0%, and a power conversion efficiency (PCE) of 7.9% as compared with those of the DSC-2, which used a J_{sc} of 17.1 mA/cm^2, V_{oc} of 0.72 V, FF of 50.0%, and PCE of 6.2%.

dx.doi.org/10.1021/jp308193y | J. Phys. Chem. C 2013, 117, 2734−2739

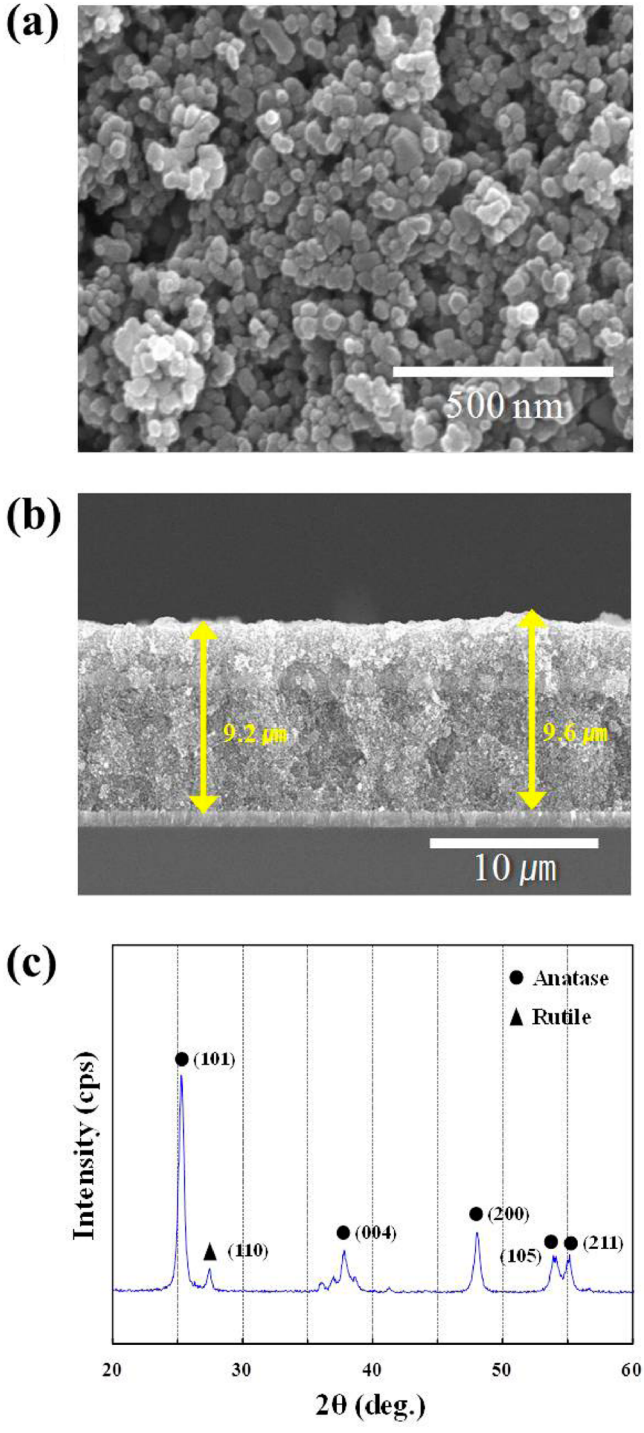

Figure 2. SEM images of the morphologies (a) and the thicknesses (b) of the TiO_2 electrodes. The XRD measurement (c) confirms the conventional anatase phase of the TiO_2 film.

The higher J_{sc} and FF of the DSC-1 are mainly attributed to a larger dye adsorption to the TiO_2 and a relatively lower series resistance (R_s),[24] while the lower V_{oc} of the DSC-1 as compared to that of the DSC-2 is attributed to a larger dark current in the junction interface between TiO_2/electrolyte because the V_{oc} is a function of the ideality factor and the dark current as a charge-transfer loss, which represents the reverse saturation current density (J_0) in general diode structure. For a quantitative analysis of the V_{oc} degradation, the *J-V* curves were fitted using the eq 1, and the parameters relating the current

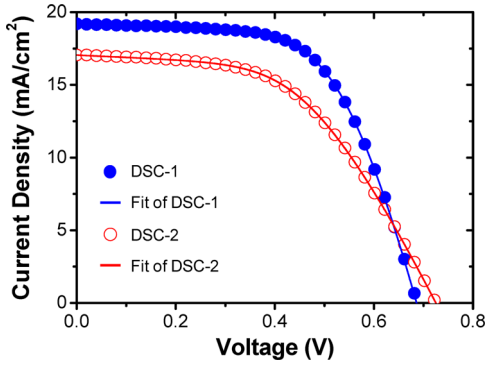

Figure 3. *J-V* characteristics under illumination and their fitting of the DSCs.

flow to the physical characteristics were extracted. The fitted curves were drawn on the experimental *J-V* characteristics using simple numerical calculations, and the resulting parameters are listed in Table 1.

The device structure of DSCs has a nearly Schottky barrier structure, which implies that the device operation should be described by the thermionic emission of charge carriers. From eq 3, A^* is calculated to be $\sim 1.2 \times 10^5$ mA/cm^2/K^2 because the effective mass (m^*) of the *anatase* TiO_2 used in this work is approximately a factor of 10 of the free electron mass (m_0).[25] Consequently, as the product of A^*T^2, the J_{00} is approximately 1.1×10^{10} mA/cm^2. From eq 2 and the extracted parameter J_0, the barrier height ($q\phi_B$) is simply calculated to be ~0.86 and 0.89 eV for DSC-1 and DSC-2, respectively. When J_0 is $\sim 1.5 \times 10^{-5}$ mA/cm^2, the barrier height of DSC-2 approaches the ideal barrier height condition of 0.9 eV, which indicates the reverse saturation current density as a native charge-transfer loss as much as $\sim 10^{-6}$ mA/cm^2, despite the ideal barrier height condition. However, the calculated barrier heights, converted to the open-circuit voltage (V_{oc}), are significantly different as compared with the real barrier heights: a V_{oc} of 0.69 and 0.72 V for DSC-1 and DSC-2, respectively. Therefore, we used the modified junction diode equation using the TED theory, as indicated in eq 4. For DSC-1, J_{00}' is $\sim 1.37 \times 10^7$ mA/cm^2 for the real barrier height of 0.69 eV, and α is calculated to be $\sim 12.5 \times 10^{-3}$. It should be noted that the J_{00}' is typically $\sim 1 \times 10^{10}$ mA/cm^2 in the electric field range 10^4 to 10^5 V/cm for a usual metal−silicone Schottky barrier system and a thousand times higher than that of DSC system. The difference of J_{00}' values between the metal−silicone system and the DSC system is quite reasonable because the electron mobility of silicone is approximately a thousand times higher than that of the *anatase* TiO_2.[25] Notably, α is a rather complicated parameter; it is necessary to include the additional loss process and its physical analysis for a subsidiary CTLF. From the extracted parameters (Table 1), the ideality factors (n) have the same values of 2.02 for DSC-1 and DSC-2. The ideality factor (n) is another important parameter in characterizing the device performance. The values of n for general *p-n* junction devices that are dominated by diffusion fall in the range of 1−2. The ideality factors obtained imply that the recombination is slightly dominant as compared with diffusion. The υ_R/υ_D term related to the residual CTLF in eq 5 is a parameter influenced by the ideality factor, and the value of υ_R/υ_D is expected to be negligible. The parameter α has approximately the same value as the product of $f_P f_Q$. Considering that the electron emission probability (f_P) approaches unity, the value of α with $\sim 12.5 \times$

dx.doi.org/10.1021/jp308193y | J. Phys. Chem. C 2013, 117, 2734−2739

Table 1. Performance Parameters and the Fitted Results Obtained from the *J-V* Characteristics of the DSCs

experimental parameters	V_{oc} (V)	J_{sc} (mA/cm^2)	FF (%)	eff. (%)	fitted results	J_0 (mA/cm^2)	ideality factor	R_s (Ω cm^2)
DSC-1	0.69	19.2	60.0	7.9		3.7×10^{-5}	2.02	5.4
DSC-2	0.72	17.1	50.0	6.2		1.5×10^{-5}	2.02	12.2

10^{-3} depends on the f_Q, which can represent current flow via quantum-mechanical tunneling and reflection as a subsidiary CTLF. Such a calculating approach based on the modified diode equation model is also applicable to DSC-2, which is calculated to have a α value of 16.1×10^{-3}.

Figure 4 illustrates the modified diode model for the DSCs described above: a conventional energy expression between

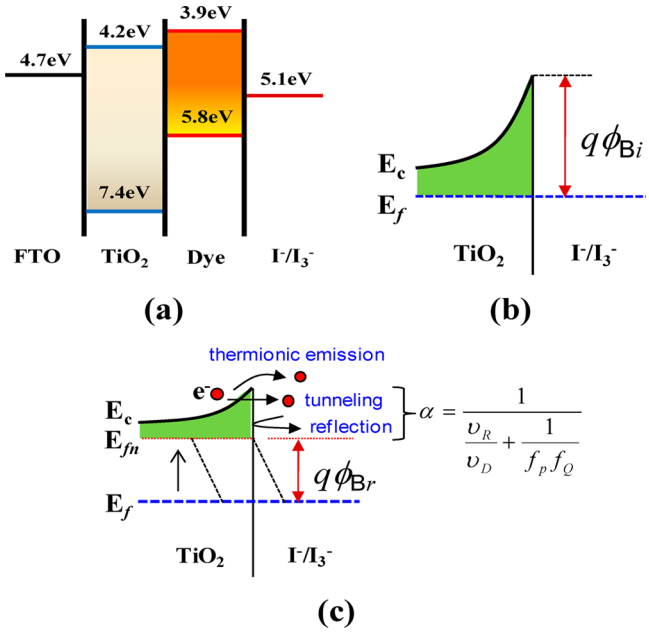

Figure 4. Modified diode model to the DSCs: a conventional energy expression between materials (a), an ideal barrier height expression extracted from the TiO_2/electrolyte junction in the equilibrium state in darkness (b), and a real barrier height expression by quasi-Fermi level splitting and the CTLFs (tunneling and reflection) in the nonequilibrium state under carrier injection (c).

materials (a),[16] an ideal barrier height expression extracted from the TiO_2/electrolyte junction in equilibrium in darkness (b), and a real barrier height expression for quasi-Fermi level splitting[26−28] and the charge-transfer process in nonequilibrium under carrier injection (c). The ideal barrier height ($q\phi_{Bi}$) in Figure 4b indicates the energy difference of 0.9 eV between TiO_2 with 4.2 eV and the electrolyte with 5.1 eV denoted in Figure 4a. In the nonequilibrium state (Figure 4c), the injected electrons with the quasi-Fermi level splitting are transported over the potential barrier and/or through the quantum-mechanical tunneling via the TED process.[20] The real barrier height ($q\phi_{Br}$) suffers a potential drop from the components of quantum-mechanical tunneling and reflection, which is the subsidiary CTLF described above. It should be noted that the current flow expressed in Figure 4c is opposite to that generated by the photovoltaic effect.[29] The real barrier height ($q\phi_{Br}$) is a figure of merit that evaluates the equivalency of the current flow via thermionic emission and that is generated via the photovoltaic effect. This latter flow includes the current flow caused by quantum-mechanical tunneling and reflection, in which the quantum-mechanical reflection of the charge carriers is a quantum reflection process of the charge carriers transported to the TiO_2 surface through the redox couple. The parameter α is a physical quantity responsible for the charge-transfer loss at the interface between TiO_2/electrolyte, which is described in the following section.

Figure 5 presents Nyquist plots and their fitting of the DSCs. The inset is an equivalent circuit of the DSCs,[30,31] where Z_1

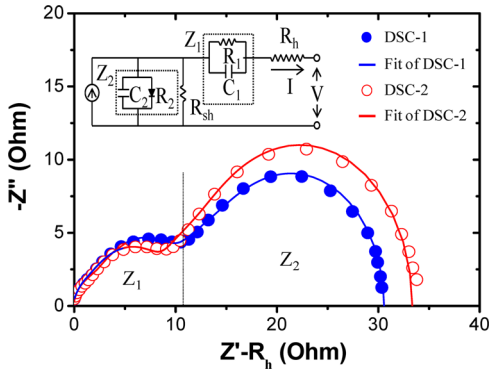

Figure 5. Nyquist plots and their DSC fittings. The inset is an equivalent circuit of the DSCs.

and Z_2 are the impedances consisting of the resistance-capacitance (RC) components described by eqs 6 and 7. R_{sh} is the shunt resistance, and R_h is the resistance of the transparent conducting oxide layer.

$$Z' = R_h + \frac{R}{1 + \omega^2 C^2 R^2} \tag{6}$$

$$-Z'' = \frac{\omega C R^2}{1 + \omega^2 C^2 R^2} \tag{7}$$

where R is the charge-transfer resistance, C is the capacitance, and ω is the angular frequency. The parameters Z_1 and Z_2 represent the impedance related to charge transport at the Pt counter electrode in the high-frequency region and the impedance related to that at the interface between the TiO_2 and the electrolyte in the middle-frequency region, respectively.

The Nyquist plots in Figure 5 are fitted in a smooth envelope using a simple combination of the RC components, in which the R_h components are excluded because the bulk resistive property is not considered in this work. From the fitted result in Figure 5, the dominant RC time constant influencing the CTLF related to the Z_1 region is roughly estimated to be ~0.25 $\times 10^{-3}$ and ~0.41 $\times 10^{-3}$ s for DSC-1 and DSC-2, respectively. Similarly, the dominant RC time constants related to the Z_2 region are also roughly estimated to be ~13.5 $\times 10^{-3}$ and ~17.1 $\times 10^{-3}$ s for DSC-1 and DSC-2, respectively. The responses extracted from the Z_2 region indicate a recombination time with oxidized redox in the TiO_2/electrolyte system.[32] In addition, the dominant RC time constants of 13.5 $\times 10^{-3}$ and 17.1 $\times 10^{-3}$ s are in good agreement with the obtained parameters α of 12.5 $\times 10^{-3}$ and 16.1 $\times 10^{-3}$ for DSC-1 and DSC-2, respectively; the product of RC time constant has a

dx.doi.org/10.1021/jp308193y | J. Phys. Chem. C 2013, 117, 2734−2739

property equivalent with charge-carrier lifetime. The larger RC time constant increases a probability of charge transfer at the interface between TiO_2/electrolyte, while the smaller RC constant increases a probability of charge-transfer loss. It is found that the parameter α as a probability has a physical quantity equivalent with time domain. The responses extracted from the Z_1 region also have a high possibility of electron transport time in the TiO_2,[33] which is an equivalent quantity with the charge-transfer loss at the Pt counter electrode.

Figure 6 presents the normalized loss factors for the DSC-1 and the DSC-2. The peaks from the normalized loss factor

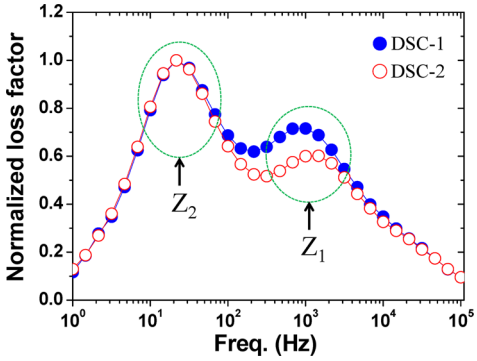

Figure 6. Normalized loss factors for the DSC-1 and the DSC-2.

represent the dominant CTLFs in the DSCs.[21] The dominant charge-transfer losses at the TiO_2/electrolyte (Z_2 region) and the Pt counter electrode (Z_1 region) occur near 25 Hz ($\sim 40 \times 10^{-3}$ s) and 1 kHz ($\sim 1 \times 10^{-3}$ s), respectively. These frequency responses are the result of the superposition of various responses, which are roughly distinguishable in Figure 5. The parameter α extracted from Figure 4 can be identified with the responses described above because α is a probability representing the behavior of the charge carriers in the TiO_2 bulk region near the interface between the TiO_2/electrolyte system. The responses from the Z_2 region originate from a charge-carrier trap site because of the defective TiO_2 surface properties; the charge carriers transported to the TiO_2 surface through the redox couple are trapped at the TiO_2 surface and recombined via the oxidized redox, which is the same mechanism of the quantum-mechanical reflection of charge carriers. In the TiO_2 bulk region near the interface between the TiO_2/electrolyte systems, the charge carriers diffuse away from the interface, where electron transport is expanded to the interface between the Pt counter electrode and the electrolyte. This transport is identified with the response from the Z_1 region.

5. CONCLUSION

In summary, we investigated the device physics of DSCs using a modified junction diode model with a Schottky barrier based on the thermionic emission-diffusion process and EIS. The parameter α obtained using the modified junction diode model and the simple *J-V* characteristic curve fitting were observed to be a physical quantity explaining the CTLFs caused at the TiO_2/electrolyte interface. The obtained parameters α of 12.5×10^{-3} and 16.1×10^{-3} are in good agreement with the dominant RC time constants of 13.5×10^{-3} and 17.1×10^{-3} s for DSC-1 and DSC-2, respectively. It is believed that the parameter α represents a physical quantity with the time domain and the dominant CTLFs at the TiO_2/electrolyte interface. It should be noted that the open-circuit voltage (V_{oc}) of DSC devices approaches the ideal V_{oc} of 0.9 V as the parameter α approaches unity. The lower V_{oc} of 0.69 V for the DSC-1 is attributed to the lower α of 12.5×10^{-3} as compared to the V_{oc} of 0.72 V for the DSC-2 with the α of 16.1×10^{-3}. In conclusion, we proved that the CTLFs obtained from the modified junction diode model can be quantified and identified as almost matching to the EIS results. In addition, we explained an origin of a degradation of V_{oc} in DSC devices using the physical model of the dominant CTLFs, which originates from the quantum-mechanical tunneling and reflection of charge carriers. Our analytical method can be applicable to provide a macroscopic evaluation for DSC device characteristics with the EIS.

AUTHOR INFORMATION

Corresponding Author

*Tel: +82 62 715 3533. Fax: +82 62 715 3464. E-mail: yjeong@gist.ac.kr (Y.J.). Tel: +82 62 715 2435. Fax: +82 62 715 2434. E-mail: shmoon@gist.ac.kr (S.-H.M.).

Notes

The authors declare no competing financial interest.

ACKNOWLEDGMENTS

This work was supported by the Core Technology Development Program for Next-generation Solar Cells of Research Institute for Solar and Sustainable Energies (RISE), GIST.

REFERENCES

(1) Grätzel, M. Photoelectrochemical Cell. *Nature* **2001**, *414*, 338−344.
(2) Grätzel, M. Solar Energy Conversion by Dye-Sensitized Photovoltaic Cells. *Inorg. Chem.* **2005**, *44*, 6841−6851.
(3) Peter, L. M. Dye-Sensitized Nanocrystalline Solar Cells. *Phys. Chem. Chem. Phys.* **2007**, *9*, 2630−2642.
(4) Hagfeldt, A.; Boschloo, G.; Sun, L.; Kloo, L.; Pettersson, H. Dye-Sensitized Solar Cells. *Chem. Rev.* **2010**, *110*, 6595−6663.
(5) Green, M. A.; Emery, K.; Hishikawa, Y.; Warta, W. Solar Cell Efficiency Tables (Version 37). *Prog. Photovoltaics: Res. Appl.* **2011**, *19*, 84−92.
(6) O'Regan, B. C.; Durrant, J. R. Kinetic and Energetic Paradigms for Dye-Sensitized Solar Cells: Moving from The Ideal to The Real. *Acc. Chem. Res.* **2009**, *42*, 1799−1808.
(7) Kopidakis, N.; Benkstein, K. D.; Van de Lagemaat, J.; Frank, A. J. Transport-Limited Recombination of Photocarriers in Dye-Sensitized Nanocrystalline TiO_2 Solar Cells. *J. Phys. Chem. B* **2003**, *107*, 11307−11315.
(8) Gledhill, S. E.; Scott, B.; Gregg, B. A. Organic and Nano-structured Composite Photovoltaics: An Overview. *J. Mater. Res.* **2005**, *20*, 3167−3179.
(9) (a) Thavasi, V.; Renugopalakrishnan, V.; Jose, R.; Ramakrishna, S. Controlled Electron Injection and Transport at Materials Interfaces in Dye Sensitized Solar Cells. *Mater. Sci. Eng., R* **2009**, *63*, 81−99. (b) Robertson, N. Optimizing Dyes for Dye-Sensitized Solar Cells. *Angew. Chem., Int. Ed.* **2006**, *45*, 2338−2345.
(10) Snaith, H. J.; Schmidt-Mende, L. Advances in Liquid-Electrolyte and Solid-State Dye-Sensitized Solar Cells. *Adv. Mater.* **2007**, *19*, 3187−3200.
(11) O'Regan, B.; Durrant, J. R.; Sommeling, P. M.; Bakker, N. J. Influence of the $TiCl_4$ Treatment on Nanocrystalline TiO_2 films in Dye-Sensitized Solar Cells. 2. Charge Density Band Edge Shifts and Quantification of Recombination Losses at Short Circuit. *J. Phys. Chem. C* **2007**, *111*, 14001−14010.
(12) Xia, J.; Yanagida, S. Strategy to Improve the Performance of Dye-Sensitized Solar Cells: Interface Engineering Principle. *Sol. Energy* **2011**, *85*, 3143−3159.

(13) Shockley, W. The Theory of p-n Junctions in Semiconductors in p-n Junction Transistors. *Bell Syst. Tech. J.* **1949**, *28*, 435−489.
(14) Sah, C. T.; Noyce, R. N.; Shockley, W. Carrier Generation and Recombination in p-n Junctions and p-n Junction Characteristics. *Proc. IRE* **1957**, *45* (9), 1228−1243.
(15) Bethe, H. A. Theory of the Boundary Layer of Crystal Rectifiers. *MIT Radiat. Lab. Rep.* **1942**, *43*, 12.
(16) Nazeeruddin, M. K.; Zakeeruddin, S. M.; Lagref, J.-J.; Liska, P.; Comte, P.; Barolo, C.; Viscardi, G.; Schenk, K.; Grätzel, M. Stepwise Assembly of Amphiphilic Ruthenium Sensitizers and Their Applications in Dye Sensitized Solar Cell. *Coord. Chem. Rev.* **2004**, *248*, 1317−1328.
(17) Cahen, D.; Hodes, G.; Grätzel, M.; Guillemoles, J. F.; Riess, I. Nature of Photovoltaic Action in Dye-Sensitized Solar Cells. *J. Phys. Chem. B* **2000**, *104*, 2053−2059.
(18) Boschloo, G.; Hagfeldt, A. Photoinduced Absorption Spectroscopy as a Tool in The Study of Dye-Sensitized Solar Cells. *Inorg. Chim. Acta* **2008**, *361*, 729−734.
(19) Crowell, C. R.; Sze, S. M. Current Transport in Metal-Semiconductor Barriers. *Solid-State Electron.* **1966**, *9*, 1035−1048.
(20) Sze, S. M. *Physics of Semiconductor Devices*, 2nd ed.; Wiley Inc.: New York, 1981; pp 259−291.
(21) Kim, B.; Lee, J.; Yu, I. Electrical Properties of Single-Wall Carbon Nanotube and Epoxy Composites. *J. Appl. Phys.* **2003**, *94*, 6724−6728.
(22) Park, D.-W.; Choi, Y.-K.; Hwang, K.-J.; Lee, J.-W.; Park, J. K.; Jang, H. D.; Park, H.-S.; Yoo, S.-J. Nanocrystalline TiO_2 Films Treated with Acid and Base Catalysts for Dye-Sensitized Solar Cells. *Adv. Powder Technol.* **2011**, *22*, 771−776.
(23) Park, D.-W.; Park, K.-H.; Lee, J.-W.; Hwang, K.-J.; Choi, Y.-K. Hydrochloric Acid Treatment of TiO_2 Electrode for Quasi-Solid-State Dye-Sensitized Solar Cells. *J. Nanosci. Nanotechnol.* **2007**, *7*, 3722−3726.
(24) Chiba, Y.; Islam, A.; Watanabe, Y.; Komiya, R.; Koide, N.; Han, L. Dye-Sensitized Solar Cells with Conversion Efficiency of 11.1%. *Jpn. J. Appl. Phys.* **2006**, *45*, 638−640.
(25) Enright, B.; Fitzmaurice, D. Spectroscopic Determination of Electron and Hole Effective Masses in a Nanocrystalline Semiconductor Film. *J. Phys. Chem.* **1996**, *100*, 1027−1035.
(26) Bisquert, J.; Cahen, D.; Hodes, G.; Ruhle, S.; Zaban, A. Physical Chemical Principles of Photovoltaic Conversion with Nanoparticulate, Mesoporous Dye-Sensitized Solar Cells. *J. Phys. Chem. B* **2004**, *108*, 8106−8118.
(27) Bisquert, J.; Vikhrenko, V. S. Interpretation of The Time Constants Measured by Kinetic Techniques in Nanostructured Semiconductor Electrodes and Dye-Sensitized Solar Cells. *J. Phys. Chem. B* **2004**, *108*, 2313−2322.
(28) Wang, P.; Zakeeruddin, S. M.; Moser, J.; Grätzel, M. A New Ionic Liquid Electrolyte Enhances the Conversion Efficiency of Dye-Sensitized Solar Cells. *J. Phys. Chem. B* **2003**, *107*, 13280−13285.
(29) Boix, P. P.; Guerrero, A.; Marchesi, L. F.; Garcia-Belmonte, G.; Bisquert, J. Current-Voltage Characteristics of Bulk Heterojunction Organic Solar Cells: Connection Between Light and Dark Curves. *Adv. Energy Mater.* **2011**, *1*, 1073−1078.
(30) Han, L.; Koide, N.; Chiba, Y.; Mitate, T. Modeling of an Equivalent Circuit for Dye-Sensitized Solar Cells. *Appl. Phys. Lett.* **2004**, *84*, 2433−2435.
(31) Fabregat-Santiago, F.; Bisquert, J.; Palomares, E.; Otero, L.; Kuang, D.; Zakeeruddin, S. M.; Grätzel, M. Correlation Between Photovoltaic Performance and Impedance Spectroscopy of Dye-Sensitized Solar Cells Based on Ionic Liquids. *J. Phys. Chem. C* **2007**, *111*, 6550−6560.
(32) Huang, S. Y.; Schlichthörl, G.; Nozik, A. J.; Grätzel, M.; Frank, A. J. Charge Recombination in Dye-Sensitized Nanocrystalline TiO_2 Solar Cells. *J. Phys. Chem. B* **1997**, *101*, 2576−2582.
(33) Enache-Pommer, E.; Boercker, J. E.; Aydil, E. S. Electron Transport and Recombination in Polycrystalline TiO_2 Nanowire Dye-Sensitized Solar Cells. *Appl. Phys. Lett.* **2007**, *91*, 123116.